Inorganic Chemistry

Article

pubs.acs.org/IC

Raman and IR Studies of Pressure- and Temperature-Induced Phase Transitions in $[(CH_2)_3NH_2][Zn(HCOO)_3]$

Mirosław Mączka,*[,†] Tercio Almeida da Silva,[‡] Waldeci Paraguassu,[‡] Maciej Ptak,[†] and Krzysztof Hermanowicz[†]

[†]Institute of Low Temperature and Structure Research, Polish Academy of Sciences, Box 1410, 50-950 Wrocław 2, Poland

[‡]Faculdade de Física, Universidade Federal do Paraná, 66075-110 Belém, Paraná, Brazil

Supporting Information

ABSTRACT: Temperature- and pressure-dependent studies of Raman and IR spectra have been performed on azetidinium zinc formate, $[(CH_2)_3NH_2][Zn(HCOO)_3]$. Vibrational spectra showed distinct anomalies in mode frequencies and bandwidths near 250 and 300 K, which were attributed to structural phase transitions associated with the gradual freezing of ring-puckering motions of the azetidinium cation. Pressure-dependent studies revealed a pressure-induced transition near 0.4 GPa. Raman spectra indicate that the structure of the room-temperature intermediate phase observed near 0.4 GPa is the same as the monoclinic structure observed at ambient pressure below 250 K. The second phase transition was found near 2.4 GPa. This transition has strong first-order character and is associated with strong distortion of both the zinc formate framework and azetidinium cations. The last phase transition was found near 7.0 GPa. This transition leads to lowering of the symmetry and further distortion of the zinc formate framework, whereas the azetidinium cation structure is weakly affected.

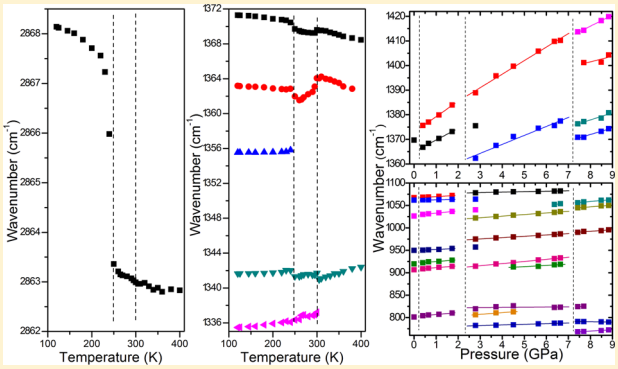

INTRODUCTION

Metal−organic frameworks (MOFs) of the general formula [cat][M(HCOO$_3$)], with M = divalent cation and cat = amine cation, have received a lot of attention in recent years because of their CO_2 sorption capacity, magnetic, ferroelectric and multiferroic properties, and glassy behavior.[1−13] In this respect, the first report on the discovery of multiferroic properties in dimethylammonium (DMA) MOFs of the formula $[(CH_3)_2NH_2][M(HCOO)_3]$ (M = Mn, Ni, Fe, Co) was published in 2009.[5] This discovery promoted broad interest in the properties and phase transition mechanism in these compounds as well as led to many efforts to synthesize novel amine-templated metal formate frameworks.[7−18]

Azetidinium metal formates ($[(CH_2)_3NH_2[M(HCOO)_3]$, AzM) with M = Mn, Cu, and Zn, crystallize in the orthorhombic structure with space group *Pnma* and undergo phase transitions into the monoclinic structures.[3,19,20] For AzZn, the transition occurs at 255 K to the $P2_1/c$ structure.[20] These compounds were also reported to exhibit giant dielectric anomalies.[19,20] Here it is important to note that AzZn is unique in the family of azetidinium metal formates because it shows the presence of an intermediate polar orthorhombic phase with space group $Pna2_1$, stable between T_{c2} = 255 and T_{c1} = 300 K.[20] Although there is no confirmation that the $Pna2_1$ phase is ferroelectric, it was suggested that the dielectric properties of this material might be related to the formation of small ferroelectric domains near T_{c1}.[20] AzM compounds with M = Cu, Zn, and Mn have also attracted attention because of the high flexibility of their frameworks, which is advantageous for creating novel ferroelastics exhibiting large shear strains.[21,22] The high flexibility of the AzMn framework was confirmed by a small value of the Young's modulus, which is less than half of the Young's modulus measured for the guanidinium analogue.[21,22]

Temperature-induced phase transitions were studied in AzM compounds by means of X-ray diffraction, NMR, differential scanning calorimtry and dielectric data.[19−21,23] These studies showed that, in the high-temperature *Pnma* phases, the azetidinium cations (Az^+) are planar, whereas they adopt a ring-puckered conformation in the low-temperature phases.[19−21,23]

Pressure-induced phase transitions in this family of MOFs were reported only for $[NH_4][Zn(HCOO)_3]$ and $[ND_4][Zn(DCOO)_3]$, possessing chiral framework of $4^9\cdot6^6$ topology and perovskite-like $[C(NH_2)_3][Mn(HCOO)_3]$ and AzMn.[22,24] The phase transition pressure was found to be only 0.41−0.66 GPa for AzMn, and it was shown that the high-pressure phase of AzMn at room temperature has the same monoclinic structure (space group $P2_1/n$) as the ambient pressure low-temperature phase stable below 273 K.[22]

Received: October 2, 2014
Published: November 14, 2014

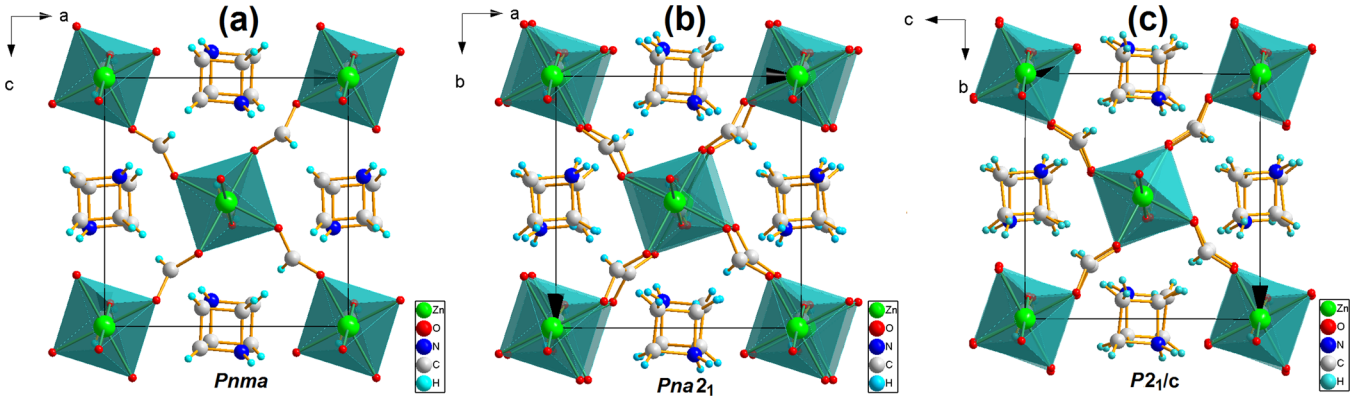

Figure 1. Structure of AzZn (a) at 308 K (*Pnma*, viewed along the *b* axis), (b) at 273 K ($Pna2_1$, viewed along the *c* axis), and (c) at 226 K ($P2_1/c$, viewed along the *a* axis). The figures were prepared by using the crystallographic data reported by Imai et al.[20]

Although temperature-induced phase transitions in AzM compounds have already been studied, the detailed mechanism of the phase transitions in AzZn is still not fully understood. Herein we analyze temperature-dependent Raman and IR data of AzZn in order to obtain deeper insight into the mechanism of the temperature-induced phase transitions in this compound. We also present high-pressure Raman data for AzZn in order to obtain information on the stability of this compound under pressure and the mechanism of the pressure-induced phase transitions. Vibrational spectroscopy is especially suited for such purposes because it is a good probe for local structure as well as studies of hydrogen bonds, displacive character, and order–disorder phase transitions.[25−27]

EXPERIMENTAL SECTION

Synthesis. Zinc perchlorate hexahydrate (Aldrich), azetidine (98%, Aldrich), methanol (99.8%, Aldrich), and formic acid (98%, Fluka) were commercially available and were used without further purification. $[(CH_2)_3NH_2][Zn(HCOO)_3]$ was obtained by a slow diffusion method. In a typical experiment, a 10 mL methanol solution containing 6.25 mmol of azetidine and 6.25 mmol of formic acid was placed at the bottom of a glass tube (5 mm inner diameter). To this solution was gently added a 16 mL methanol solution containing 2 mmol of $Zn(ClO_4)_2{\cdot}6H_2O$. The tube was sealed and kept undisturbed. Colorless crystals were harvested after 5 days. The yield was about 55% based on the starting zinc salt. The product was washed with methanol and dried at 60 °C. A good match of its powder X-ray diffraction pattern with the simulation from the single-crystal structure reported at 308 K[20] confirmed the phase purity of the obtained crystals (see Figure S1 in the Supporting Information, SI).

Raman and IR Studies. Temperature-dependent Raman spectra in the 100–3300 cm^{-1} range were measured using a Bruker FT 100/S spectrometer with YAG:Nd laser excitation (1064 nm) and a Linkam cryostat cell (THMS 600). Additional low-frequency Raman spectra in the 20–350 cm^{-1} range were measured using a Renishaw InVia Raman spectrometer equipped with confocal DM 2500 Leica optical microscope, a thermoelectrically cooled charge-coupled detector, and a diode laser operating at 830 nm. Temperature-dependent IR spectra were measured for the sample in KBr pellets in the range of 3800–400 cm^{-1} and in an Apiezon N suspension in the range of 500–50 cm^{-1} with the Biorad 575C FT-IR spectrometer using a helium-flow Oxford cryostat. The resolution of the Raman and IR spectra was 2 cm^{-1}.

The high-pressure Raman spectra were recorded using a microscope attached to a Jobin Yvon T64000 triple-grating spectrometer on about 15-μm-thick platelets of AzZn single crystals through backscattering geometry. The 514 nm line of a solid-state ion laser was used for excitation, and the spectrometer slits were set for a resolution of 2 cm^{-1}. No analyzer was used in the high-pressure experiment. In order to reach high pressures, the samples were loaded into a diamond-anvil cell μ-scope DAC HT(S) from Almax easyLab with a diamond of 0.4 mm culets. A stainless steel gasket with a thickness of 200 μm was preindented to 50 μm, and a 100 μm hole was drilled in the center of the indentation by using an electric discharge machine from Almax easyLab. The Nujol mull served as the pressure-transmitting media. Pressures were measured based on the shifts of the ruby R1 and R2 fluorescence lines.

RESULTS AND DISCUSSION

Vibrational Studies: Selection Rules and Assignment of the Modes. To understand the vibrational properties of AzZn and the mechanisms of the temperature- and pressure-induced phase transitions, it is important to discuss shortly the crystal structure of this compound. The structure is composed of ZnO_6 octahedra connected by the formate ligands and Az^+ cations located in large cavities of the zinc formate framework (see Figure 1). In the room-temperature *Pnma* structure, there are three crystallographically independent Zn–O bond lengths, one independent Az^+ cation located on the mirror plane, and one independent $HCOO^-$ anion.[20] In the $Pna2_1$ structure, there are still one independent Zn^{2+} ion and an Az^+ ion, but the number of independent $HCOO^-$ ions and Zn–O bond lengths increases to three and six, respectively.[20] Furthermore, the Az^+ ion adopts a ring-puckered conformation. In the $P2_1/c$ structure, the number of independent Zn^{2+} ions increases to two.[20]

The vibrational modes of AzZn can be subdivided into internal vibrations of the azetidinium and formate ions and lattice vibrations. Table S1 in the SI shows the correlation between the optical modes in the *Pnma*, $Pna2_1$, and $P2_1/c$ structures of AzZn. The experimental wavenumbers for AzZn are presented in Table S2 in the SI.

The Raman and IR spectra of the studied compounds are presented in Figures 2 and 3 and S2–S5 in the SI. The assignment of bands corresponding to internal vibrations of the $HCOO^-$ ions is straightforward because these bands appear in narrow-wavenumber ranges[11,16,17] and will not be discussed here. As far as Az^+ is concerned, the free ion should have 30 internal vibrations that can be subdivided into vibrations of the NH_2 and CH_2 groups as well as ring vibrations (see Table S1 in the SI). Although assignment of the modes for Az^+ is not reported in the literature, there are a few papers discussing assignment of the modes for free Az molecules based on density functional theory (DFT) calculations.[28] Furthermore, our previous IR and Raman studies of MOFs containing DMA^+ and formamidinium cations showed that vibrations of the NH_2

dx.doi.org/10.1021/ic502426x | Inorg. Chem. 2014, 53, 12650–12657

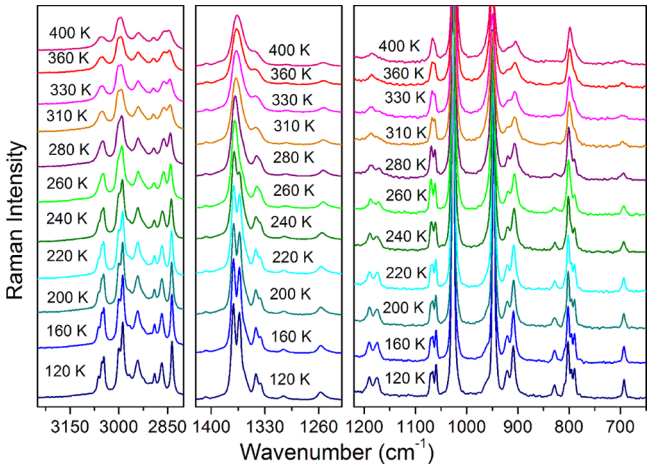

Figure 2. Enlarged parts of the Raman spectra showing details in the spectral ranges 2800−3250, 1230−1420, and 650−1220 cm^{-1}.

groups usually give rise to strong IR bands and weak Raman bands, whereas the opposite holds for the C−H vibrations.[11,16] Having this in mind and taking into account the results of DFT calculations for azetidine, the majority of internal modes of Az^+ can be easily assigned, as proposed in Table S1 in the SI. There are, however, a few bands that are more difficult to assign. First, according to the DFT calculations for Az molecules, $\delta(CH_2)$ modes are observed at 1445−1499 cm^{-1}.[28] We assign, therefore, the bands of AzZn in the 1439−1477 cm^{-1} region to $\delta(CH_2)$. However, our spectra show two additional weak bands at 1406 and 1395 cm^{-1}. Weak bands in this frequency range were previously observed by us for DMA metal formates and assigned to $\omega(NH_2)$ and $\tau(NH_2)$.[11] We suppose, therefore, that the discussed bands of AzZn may also correspond to $\omega(NH_2)$ and $\tau(NH_2)$. Second, studies of DMA metal formates showed that $\rho(NH_2)$ is usually observed as a broad band near 900−935 cm^{-1} at room temperature, which exhibits pronounced narrowing upon cooling.[11] A similar band is observed at 1083 cm^{-1} for formamidinium manganese formate.[16] Our IR spectra show that a band at 865 cm^{-1} is hardly visible at room temperature but clear at low temperatures because of significant narrowing. We suppose that this band can be assigned to the $\rho(NH_2)$ mode. Third, DFT calculations predict that the ring-puckering mode corresponds to the Raman (IR) band observed for azetidine at 217 cm^{-1} (207 cm^{-1}).[28,29] However, the calculations show that the intensity of these IR and Raman bands is weak, an order of magnitude smaller than the $\nu(CH_2)$ bands.[28] We suppose, therefore, that ring-puckering modes contribute to the Raman and IR bands observed near 200 cm^{-1} but the main contribution to the strong Raman bands comes from librational motions of $HCOO^-$ because similar strong bands in this frequency range were previously observed also for DMA, ammonium, and formamidinium metal formates.[11,16,17] On the other hand, the far-IR spectrum of AzZn is very similar to the spectrum of DMA zinc formate, and thus the most intense IR bands in the 150−420 cm^{-1} range can be attributed to translational motions of Zn^{2+} and $HCOO^-$ ions.[11]

Temperature-Dependent Raman and IR Studies: Mechanism of the Phase Transitions. Figures 2 and 3 and S2 and S3 in the SI show that, at elevated temperatures, the Raman and IR bands corresponding to the internal modes of the anionic framework exhibit much smaller bandwidths than the bands assigned to vibrations of the NH_2 group. Very large bandwidths are also observed for the lattice modes (see Figures S3 and S5 in the SI). This behavior confirms the presence of disorder and formation of hydrogen bonds between Az^+ and the framework that was reported previously using the X-ray diffraction method.[20] Upon cooling, the bandwidth changes weakly down to room temperature. Nevertheless, when the temperature decreases below 300 K, some new bands become clearly evident (see Table S2 in the SI). For instance, the Raman band at 1342 cm^{-1} clearly splits into a doublet below 300 K. The appearance of new bands indicates the onset of the *Pnma*-to-$Pna2_1$ phase transition. Upon a further decrease of the temperature, the lattice bands exhibit an abrupt narrowing near 250 K (see Figure S3 in the SI). The temperature at which this behavior is observed corresponds well with the T_{c2} temperature of the $Pna2_1$-to-$P2_1/c$ phase transition. A further decrease in the bandwidth and separation between the split components become evident when the temperature decreases to 80 K (Raman) and 5 K (IR).

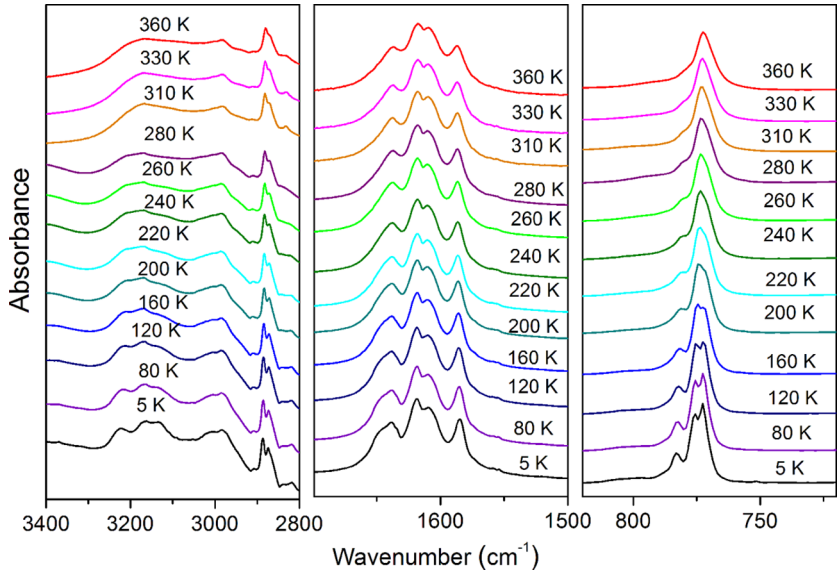

Figure 3. Details of the IR spectra results corresponding to the spectral ranges 2800−3400, 1500−1700, and 720−820 cm^{-1} for AzZn.

dx.doi.org/10.1021/ic502426x | *Inorg. Chem.* 2014, 53, 12650−12657

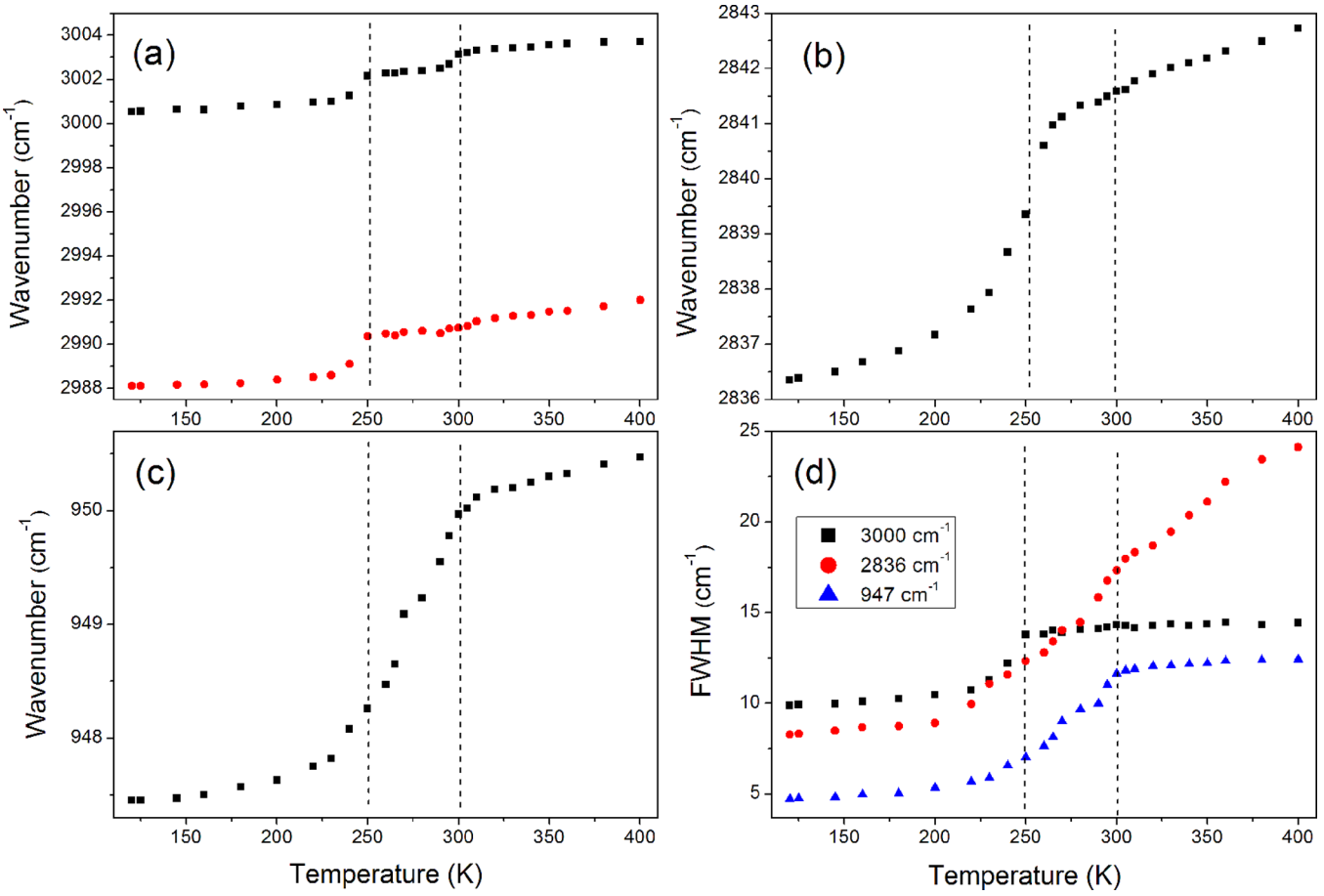

Figure 4. Temperature evolution of (a and b) $\nu(CH_2)$ and (c) ring-stretch Raman frequencies of AzZn. (d) Temperature evolution of fwhm of the 3000 and 2836 cm^{-1} [$\nu(CH_2)$] and 947 cm^{-1} (ring stretch) Raman bands of AzZn. The vertical lines indicate temperatures of the phase transitions.

To observe the changes at the phase transitions more clearly, we present temperature evolution of Raman frequencies and full width at half-maximum (fwhm) values for some selected modes (see Figures 4 and S6 in the SI). Figure 4 shows that the $\nu(CH_2)$ modes of Az^+ exhibit nearly no anomalies at the *Pnma*-to-*Pna*2_1 phase transition near 300 K. Very significant, gradual decreases in the frequency and fwhm at this transition are, however, observed for the ring stretch of Az^+. This type of behavior is consistent with an order−disorder phase transition associated with freezing of the ring-puckering motion of Az^+, as reported on the basis of X-ray diffraction.[20] In contrast to X-ray diffraction data, which showed an abrupt change of the ring-pucker angle to about 17° near 300 K, followed by a much weaker increase of this angle up to about 24° upon cooling to 255 K, Raman and IR data suggest a more gradual freezing of the ring-puckering motion below 300 K. Figure S6 in the SI shows that the internal modes of $HCOO^-$ ions also exhibit a significant and gradual decrease in fwhm below 300 K. This behavior is yet another confirmation that the phase transition near 300 K is governed by the ring-puckering dynamics of Az^+. Figure S6b in the SI shows, however, that the *Pnma*-to-*Pna*2_1 phase transition is also associated with weak distortion of the framework.

The *Pna*2_1-to-*P*$2_1/c$ phase transition near 250 K has significantly different character. First, this transition has strongly first-order nature, as evidenced by abrupt changes in the bandwidths of the lattice modes and the frequencies of the $HCOO^-$ modes (see Figures S3 and S6 in the SI). Second, the distortion of the framework is more pronounced, as evidenced by larger shifts of $HCOO^-$ frequencies at this phase transition. Interestingly, the $\nu_1(HCOO^-)$ mode exhibits about a 4 cm^{-1} upshift at the *Pna*2_1-to-*P*$2_1/c$ phase transition, although no anomaly was observed for this mode at the *Pnma*-to-*Pna*2_1 phase transition (see Figure S6a in the SI). Upshifts are also observed for nearly all $\nu_2(HCOO^-)$ and $\nu_5(HCOO^-)$ modes, in contrast to downshifts observed at the *Pnma*-to-*Pna*2_1 phase transition. Such behavior indicates that the C−H and C−O bonds in the $HCOO^-$ ions exhibit a shortening in the *P*$2_1/c$ phase. Third, the fwhm values of the ring-stretching and $HCOO^-$ internal modes exhibit large decreases in the 250−300 K range but change weakly below 250 K. This behavior indicates that the freezing of ring-puckering motions is nearly complete near 250 K. This result is consistent with the X-ray diffraction data that revealed a constant value of the ring-pucker angle below approximately 250 K.[20] Interestingly, very pronounced changes in fwhm below 250 K of the lattice modes suggest that some amount of thermally activated motion is retained by the Az^+ cation even in the monoclinic phase. Figure 4 also shows that the phase transition near 250 K is associated with very pronounced changes in the fwhm values and frequencies of the $\nu(CH_2)$ modes. This behavior suggests that the dynamics of the CH_2 groups play a significant role in the mechanism of the *Pna*2_1-to-*P*$2_1/c$ phase transition.

In summary, Raman and IR data show that at very low temperatures the motions of the Az^+ cations are frozen, and according to the X-ray diffraction data, Az^+ adopts a ring-

dx.doi.org/10.1021/ic502426x | *Inorg. Chem.* 2014, 53, 12650−12657

puckered configuration. Upon heating, the motions of the CH_2 groups and the azetidinium ring become thermally activated. When the temperature reaches about 250 K, the hydrogen bonds between Az^+ and the framework are not able to overcome thermally activated motions and, as a result, a phase transition into the $Pna2_1$ phase occurs. Upon a further increase in the temperature, the thermally activated ring-puckering motions become very pronounced, and at about 300 K, a second phase transition into the *Pnma* structure occurs, in which Az^+ ions adopt a planar conformation. Thus, similar to other amine-templated metal formates, the phase transition mechanisms seem to be mainly related with the thermally activated dynamical motion of the organic cations. However, order−disorder changes of the organic cations are associated with some distortion of the framework. In the AzZn studied here, this distortion is weak, as evidenced by small shifts of the internal modes at the phase transition temperatures (less than 4 cm^{-1}). Much larger distortion was observed previously for DMA (some internal modes of $HCOO^-$ exhibited a shift up to 15 cm^{-1}) and formamidinium analogues (a shift up to 8 cm^{-1}).[11,16]

High-Pressure Raman Scattering Study and Mechanism of the Pressure-Induced Phase Transition. The pressure-dependent Raman spectra are presented in Figure S7 in the SI. Figure 5 shows the pressure dependence of the wavenumbers, which can be well described using linear function $\omega(P) = \omega_0 + \alpha P$. Table 1 summarizes values of the wavenumber intercepts at zero pressure (ω_0) and pressure coefficients ($\alpha = d\omega/dP$), obtained from fitting of the experimental data by the linear function.

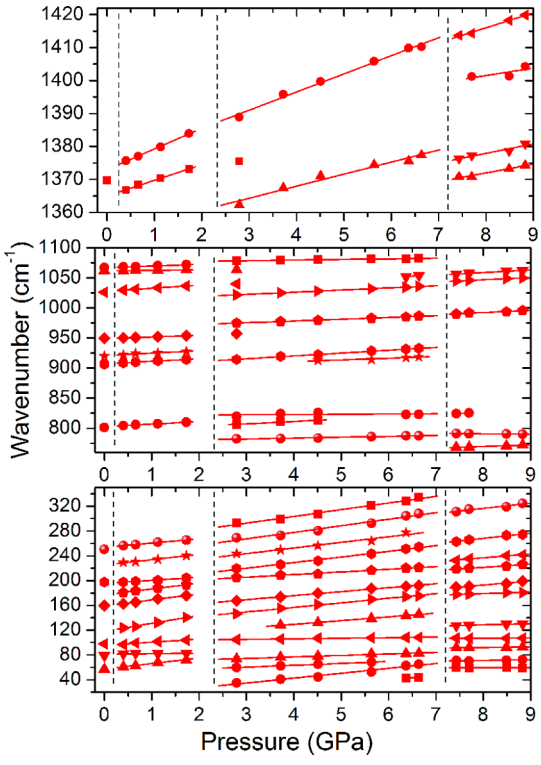

Figure 5. Wavenumber versus pressure plots of the Raman modes observed in the AzZn crystal for the compression experiment. The solid lines are linear fits on the data to $\omega(P) = \omega_0 + \alpha P$. The vertical lines show the pressures at which structural phase transitions occur.

When the pressure increases, the spectrum exhibits significant changes at 0.4 GPa (see Figure S7 in the SI). The most characteristic changes are (i) splitting of the lattice bands into a few narrower components and (ii) splitting of the 1370 cm^{-1} band into a doublet (Figures 5 and S7 in the SI). The observed changes in the Raman spectra are very similar to those observed at ambient pressure upon cooling below 250 K. Our results indicate therefore that AzZn undergoes near 0.4 GPa a phase transition into the $P2_1/c$ structure (intermediate phase I), which is observed at ambient pressure below 250 K. This result shows that dT_{c2}/dP is larger than about 100 K GPa^{-1}. This value is very large and even larger than the 46 K GPa^{-1} value expected for $[(CH_3)_2NH_2][Mn(HCOO)_3]$.[30] As mentioned already in the Introduction, for AzMn analogue the transition into the monoclinic phase was also observed at very low pressure, that is, at 0.41−0.66 GPa.[22] Thus, our result confirms very high flexibility of the AzM frameworks and shows that the first pressure-induced phase transition is associated with the freezing of ing-puckering motions.

Upon a further increase of pressure, the spectra remain qualitatively the same up to 1.7 GPa and all bands exhibit the usual shift toward higher wavnumbers. Inspection of Table 1 shows that the pressure coefficients for Raman modes corresponding to internal vibrations of the $HCOO^-$ ions (bands near 1365−1373, 1062−1067, and 801 cm^{-1}), Az^+ ions (bands near 1026 and 950 cm^{-1}), and lattice modes (below 300 cm^{-1}) are 0.92−6.28, 2.8−5.0, and 0.69−12.89 cm^{-1} GPa^{-1}. As can be noticed, these values are large even for ring modes of the Az^+ cation, indicating that the application of pressure leads not only to significant changes of the framework but also to large changes in the C−C and C−N bonds of the Az ring. This behavior is significantly different from that observed for other formates such as $[NH_4][Zn(HCOO)_3]$, $[ND_4][Zn(DCOO)_3]$, and $[tmenH_2][Er(HCOO)_4]$ ($tmenH_2^{2+}$ = *N*,*N*,*N*′,*N*′-tetramethylethylenediammonium), for which experimental and theoretical studies revealed significant compressibility of the metal−oxygen polyhedra and rigidity of the organic ligands.[24,31]

When the pressure reaches 2.8 GPa, the Raman spectrum changes drastically. First of all, the bands exhibit abrupt wavenumber shifts and change in their relative intensities, some of them split, and a very strong low-frequency band appears at 35 cm^{-1} (Figures 5 and S7 in the SI). However, the spectrum at 2.8 GPa also shows the presence of weak bands corresponding to the original phase, pointing to the coexistence of two phases at this pressure. The observed modifications of the Raman spectra indicate that a first-order phase transition takes place in AzZn near 2.4 GPa. Our Raman data allow us to obtain some information on the pressure-induced structural changes in the intermediate phase II. First of all, our data show a large splitting of the $\nu_3(HCOO^-)$ mode near 800 cm^{-1} into three components (see Figure 5). This splitting indicates that the metal formate framework is very strongly distorted in the intermediate phase II. Because the $\nu_3(HCOO^-)$ mode is the symmetric O−C−O bending (scissor) mode, the observed splitting suggests the presence of three crystallographically unique $HCOO^-$ ions in this phase, with significantly different C−O bonds. This splitting changes weakly upon a further increase of the pressure, but the modes exhibit a significant shift toward higher wavenumbers. This behavior indicates that the metal formate framework distortion of the intermediate phase II changes weakly upon compression, but the C−O bonds exhibit significant compression. Another interesting observation is that the Az^+ ring-stretching modes near 950 cm^{-1} (1026

dx.doi.org/10.1021/ic502426x | *Inorg. Chem.* 2014, 53, 12650−12657

Table 1. Raman Wavenumbers ω_0 for the Two Phases of AzZn along with Pressure Coefficients α Obtained from the Linear Fits on the Data to $\omega(P) = \omega_0 + \alpha P$

ambient pressure phase	intermediate phase I		intermediate phase II		high-pressure phase		
ω (cm^{-1})	ω_0 (cm^{-1})	α (cm^{-1} GPa^{-1})	ω_0 (cm^{-1})	α (cm^{-1} GPa^{-1})	ω_0 (cm^{-1})	α (cm^{-1} GPa^{-1})	assignment
			23.1	3.11	60.9	−0.21	L($HCOO^-$)
			11.1	7.88	62.8	1.04	L($HCOO^-$)
			51.2	3.02			L($HCOO^-$)
56.8	57.1	8.90	67.4	2.37	84.9	0.88	L($HCOO^-$)
79.0	81.5	0.69					L($HCOO^-$)
97.8	95.5	5.01	102.5	0.90	105.7	0.16	L($HCOO^-$)
			105.7	5.94	113.0	1.94	L($HCOO^-$)
	118.1	12.89	127.1	7.40	160.6	2.30	L($HCOO^-$)
159.4	158.8	9.93	149.8	6.46	140.0	6.61	L($HCOO^-$)
	177.1	9.43	192.8	4.23	179.7	5.21	L($HCOO^-$)
					185.5	6.41	L($HCOO^-$)
197.4	195.5	4.93	192.4	9.15	201.1	8.38	L($HCOO^-$)
	225.3	8.50	216.4	9.05			T′($HCOO^-$)
250.4	253.8	6.76	235.8	10.54	249.4	8.39	T′(Zn^{2+}) and T′($HCOO^-$)
			260.2	10.86			T′(Zn^{2+}) and T′($HCOO^-$)
					747.4	2.77	ν_3($HCOO^-$)
			777.8	1.45	797.1	−0.79	ν_3($HCOO^-$)
			795.9	3.78			ν_3($HCOO^-$)
801.1	802.6	4.29	821.3	0.81	797.3	3.63	ν_3($HCOO^-$)
			899.9	2.74			ring stretch
906.4	907.2	4.06	901.4	4.73			ring stretch
919.6	921.0	3.93					ring stretch
949.7	949.0	2.80	966.6	2.93	963.9	3.55	ring stretch
1026.2	1027.8	5.00	1011.8	3.58	1017.1	3.72	ring stretch
			1011.0	6.44	1024.5	4.29	ring stretch
1061.7	1061.6	0.92					ν_6($HCOO^-$)
1067.2	1066.9	2.85	1075.5	1.01			ν_6($HCOO^-$)
					1350.8	2.64	ν_2($HCOO^-$)
			1353.3	3.65	1354.9	2.88	ν_2($HCOO^-$)
1369.7	1365.0	4.72			1383.2	2.28	ν_5($HCOO^-$)
	1373.0	6.28	1374.5	5.51	1379.6	4.56	ν_5($HCOO^-$)

cm^{-1}) exhibit a strong upshift (downshift) at the phase transition by about 20 cm^{-1} (17 cm^{-1}). Such a pronounced change indicates that the phase transition is associated with a large change in the conformation of the Az^+ cation. It is also worth noting that the strong band at 35 cm^{-1}, which appears at 2.7 GPa, shows strong pressure dependence; that is, the pressure coefficient α is 7.88 GPa cm^{-1} and the ω_0 value is very small, only 11.1 cm^{-1}. The strong intensity of this mode suggests that it is related to librational motions of $HCOO^-$ ions. On the other hand, the very small value of ω_0 suggests that this mode behaves as a soft mode in this intermediate phase II. Thus, our results suggest that the phase transition near 2.4 GPa has a displacive character and is associated with the instability of librational motions of formate ions. Table 1 also shows that most of the Raman bands of the intermediate phase II still exhibit a strong pressure dependence, pointing to the large compressibility of this phase.

When the pressure changes from 6.6 to 7.4 GPa, the Raman spectrum again exhibits significant changes. In particular, the bands near 1370 and 1410 cm^{-1}, attributed to the $\nu_2(HCOO^-)$ and $\nu_5(HCOO^-)$ modes, split into doublets, and the intensity of the former band strongly increases. Furthermore, an additional component of the $\nu_3(HCOO^-)$ mode appears at 768 cm^{-1}, and the intensity of the low-frequency band at 65 cm^{-1} (at 6.6 GPa), which corresponds to the librational mode of $HCOO^-$, strongly decreases (see Figure S7 in the SI). Contrary to large changes observed for the $HCOO^-$ modes, the modes of the azetidinium cation exhibit weak changes at the phase transition. Raman data indicate, therefore, that the phase transition near 7.0 GPa is associated with significant distortion of the zinc formate framework, whereas the structure of the azetidinium cation is weakly affected. The above-discussed splitting of the $HCOO^-$ modes into doublets points to a decrease in the symmetry of the high-pressure phase. It is worth noting, however, that the Raman bands at 8.8 GPa are still relatively narrow, indicating no amorphization of AzZn up to 8.8 GPa. This behavior is significantly different from that observed for $[ND_4][Zn(DCOO)_3]$, which exhibited partial amorphization already near 4 GPa.[24]

Raman spectra of AzZn during decompression are presented in Figure S8 in the SI. The observed changes in the Raman spectra are similar to those observed upon compression, indicating reversibility of the phase transitions. However, the phase transition pressure into the intermediate phase II is lower (about 6.4 GPa) than that upon compression (about 7.0 GPa). Significant hysteresis can be attributed to the first-order nature of this transition.

Our Raman data show that AzZn is a very soft material that exhibits significant compression of the C−O and Zn−O bonds of the framework as well as the Az^+ cation. The induced in this way increase of the hydrogen-bond strength between the Az^+ and the framework leads to the freezing of ring-puckering

dx.doi.org/10.1021/ic502426x | Inorg. Chem. 2014, 53, 12650−12657

motions and the structural change into the monoclinic phase. This transition occurs at low pressure (near 0.4 GPa), and the structure of this intermediate phase I is isostructural to the low-temperature one observed at ambient pressure. Upon a further increase of the pressure, the size of the cavity occupied by Az^+ decreases further, leading to an increase in the hydrogen-bond strength and repulsion forces between the oxygen atoms. When the pressure reaches about 2.4 GPa, the structure becomes unstable and a strong first-order phase transition takes place, which is associated with rotations of the $HCOO^-$ ions and their distortion. These changes are associated with large changes in the hydrogen-bond network and structure of the azetidinium cation. The splitting of some bands points to the low symmetry of the intermediate phase II. When the pressure increases to 7.0 GPa, AzZn experiences the third pressure-induced phase transition. Our data show that this transition is also associated with lowering of the crystal symmetry and distortion of the zinc formate framework. In contrast to the phase transition near 2.4 GPa, the transition near 7.0 GPa does not lead to any significant changes in the structure of the Az^+ cation. It is worth noting that recent experimental studies of a few amine-templated metal formates revealed that the high-pressure structural changes in these compounds usually lead to a large change in the metal−oxygen coordination sphere and rotation of the rigid organic ions.[24,31] For instance, studies of $[tmenH_2][Er(HCOO)_4]$ showed that the pressure-induced phase transition in this compound is associated mainly with significant distortion of the Er−O polyhedra, whereas the organic cation does not play any significant role in the phase transformation.[31] Our data show very different behavior; that is, the Az^+ cation certainly plays a very significant role in the pressure-induced phase transition to the intermediate phases I and II. Large structural changes under pressure in this compound can most likely be attributed to the high flexibility of AzZn, as evidenced by small values of the Young's moduli for this crystal.

CONCLUSIONS

Temperature-dependent Raman and IR measurements have demonstrated dynamic disorder of the high-temperature phase of AzZn due to ring-puckering motions of the azetidinium cation. Upon cooling, the majority of the bands, especially in the lattice mode region, experience narrowing near 300 K. We have attributed this change to the onset of the structural phase transition to the phase with partially frozen ring-puckering motions. Upon a further decrease in the temperature, an abrupt decrease of the bandwidths of the lattice modes occurs near 250 K. This behavior has revealed the onset of another strong first-order phase transition to the ordered phase. Our data also showed significant anomalies near the phase transition temperatures for many internal modes of the formate ions. This behavior indicates that the ordering of the azetidinium cations is also associated with some distortion of the framework.

Pressure-dependent studies revealed that AzZn is a very soft material. It experiences three pressure-induced structural phase transitions. The first transition takes place at a very low pressure, near 0.4 GPa, to the monoclinic phase, which is observed at ambient pressure below 250 K. This monoclinic phase is also very soft and experiences a strong first-order phase transition near 2.4 GPa. The third phase transition occurs near 7.0 GPa. The structural changes in the phases stable above 2.4 GPa are associated with strong distortion of the zinc formate framework. Raman data indicate, however, that the structure of the azetidinium cation is also strongly affected by the phase transition near 2.4 GPa. Our data indicate, therefore, that these phase transitions are associated with significant rearrangement of the framework due to rotations of the $HCOO^-$ ions. The phase transition near 2.4 GPa is also associated with reorientation of the azetidinium cations, which, in turn, results in large changes in the hydrogen-bond network and Az^+ conformation.

ASSOCIATED CONTENT

Supporting Information

Powder X-ray diffraction, IR and Raman spectra, and temperature dependence of the bandwidths and frequencies (Figures S1−S8), correlation diagram showing the correspondence between the optical modes in the *Pnma*, $Pna2_1$, and $P2_1/c$ structures of AzZn (Table S1), and Raman and IR frequencies for AzZn, together with suggested assignments (Table S2). This material is available free of charge via the Internet at http://pubs.acs.org.

AUTHOR INFORMATION

Corresponding Author

*E-mail: m.maczka@int.pan.wroc.pl. Phone: +48-713954161. Fax: +48-713441029.

Author Contributions

The manuscript was written through contributions of all authors. All authors have given approval to the final version of the manuscript.

Notes

The authors declare no competing financial interest.

ACKNOWLEDGMENTS

The authors acknowledge the Brazilian National Research Council for a fellowship and Grant 401849/2013-9.

REFERENCES

(1) Rossin, A.; Chierotti, M. R.; Giambiastiani, G.; Gobetto, R.; Peruzzini, M. *CrystEngComm* **2012**, *14*, 4454−4460.
(2) Zhang, W.; Xiong, R. G. *Chem. Rev.* **2012**, *112*, 1163−1195.
(3) Wang, Z.; Zhang, B.; Otsuka, T.; Inoue, K.; Kobayashi, H.; Kurmoo, M. *Dalton Trans.* **2004**, 2209−2216.
(4) Jain, P.; Dalal, N. S.; Toby, B. H.; Kroto, H. W.; Cheetham, A. K. *J. Am. Chem. Soc.* **2008**, *130*, 10450−10451.
(5) Jain, P.; Ramachandran, V.; Clark, R. J.; Zhou, H. D.; Toby, B. H.; Dalal, N. S.; Kroto, H. W.; Cheetham, A. K. *J. Am. Chem. Soc.* **2009**, *131*, 13625−1327.
(6) Besara, T.; Jain, P.; Dalal, N. S.; Kuhns, P. L.; Reyes, A. P.; Kroto, H. W.; Cheetham, A. K. J. *Proc. Natl. Acad. Soc.U. S. A.* **2011**, *108*, 6828−6832.
(7) Sanchez-Andujar; Presedo, S.; Yanez-Vilar, S.; Castro-Garcia, S.; Shamir, J.; Senaris-Rodrigues, M. A. *Inorg. Chem.* **2010**, *49*, 1510−1516.
(8) Wang, W.; Yan, L.-Q.; Cong, J.-Z.; Zhao, Y.-L.; Wang, F.; Shen, S.-P.; Zhou, T.; Zhang, D.; Wang, S.-G.; Han, X.-F.; Sun, Y. *Sci. Rep.* **2013**, *3*, 2024.
(9) (a) Stroppa, A.; Jain, P.; Barone, P.; Marsman, M.; Perez Mato, J. M.; Cheetham, A. K.; Kroto, H. W.; Picozzi, S. *Angew. Chem., Int. Ed.* **2011**, *50*, 5847−5850. (b) Stroppa, A. *J. Phys. Conf. Ser.* **2013**, *428*, 012029. (c) Stroppa, A.; Barone, P.; Jain, P.; Perez-Mato, J. M.; Picozzi, S. *Adv. Mater.* **2013**, *25*, 2284−2290.
(10) Di Sante, D.; Stroppa, A.; Jain, P.; Picozzi, S. *J. Am. Chem. Soc.* **2013**, *135*, 18126−18130.
(11) (a) Mączka, M.; Gągor, A.; Macalik, B.; Pikul, A.; Ptak, M.; Hanuza, J. *Inorg. Chem.* **2014**, *53*, 457−467. (b) Mączka, M.; Ptak, M.;

Macalik, L. *Vib. Spectrosc.* **2014**, *71*, 98−104. (c) Mączka, M.; Zierkiewicz, W.; Michalska, D.; Hanuza, J. *Spectrochim. Acta, Part A* **2014**, *128*, 674−680.
(12) Tian, Y.; Cong, J.; Shen, S.; Chai, Y.; Yan, L.; Wang, S.; Sun, Y. *Phys. Status Solidi RRL* **2014**, *8*, 91−94.
(13) Tian, Y.; Wang, W.; Chai, Y.; Cong, J.; Shen, S.; Yan, L. *Phys. Rev. Lett.* **2014**, *112*, 017202.
(14) Mączka, M.; Pietraszko, A.; Macalik, L.; Sieradzki, A.; Trzmiel, J.; Pikul, A. *Dalton Trans.* **2014**, *43*, 17075−17084.
(15) (a) Wang, Z.; Zhang, B.; Inoue, K.; Fujiwara, H.; Otsuka, T.; Kobayashi, H.; Kurmoo, M. *Inorg. Chem.* **2007**, *46*, 437−445. (b) Xu, G. C.; Zhang, W.; Ma, X. M.; Hen, Y. H.; Zhang, L.; Cai, H. L.; Wang, Z. M.; Xiong, R. G.; Gao, S. *J. Am. Chem. Soc.* **2011**, *133*, 14948−14951.
(16) Mączka, M.; Ciupa, A.; Gągor, A.; Sieradzki, A.; Pikul, A.; Macalik, B.; Drozd, M. *Inorg. Chem.* **2014**, *53*, 5260−5268.
(17) (a) Mączka, M.; Pietraszko, A.; Macalik, B.; Hermanowicz, K. *Inorg. Chem.* **2014**, *53*, 787−794. (b) Shang, R.; Xu, G. C.; Wang, Z. M.; Gao, S. *Chem.—Eur. J.* **2014**, *20*, 1146−1158.
(18) Mączka, M.; Ptak, M.; Kojima, S. *Appl. Phys. Lett.* **2014**, *104*, 222903.
(19) Zhou, B.; Imai, Y.; Kobayashi, A.; Wang, Z. M.; Kobayashi, H. *Angew. Chem., Int. Ed.* **2011**, *50*, 11441−11445.
(20) Imai, Y.; Zhou, B.; Ito, Y.; Fijimori, H.; Kobayashi, A.; Wang, Z. M.; Kobayashi, H. *Chem.—Asian J.* **2012**, *7*, 2786−2790.
(21) Li, W.; Zhang, Z.; Bithell, E. G.; Batsanov, A. S.; Barton, P. T.; Saines, P. J.; Jain, P.; Howard, C. J.; Carpeneter, M. A.; Cheetham, A. K. *Acta Mater.* **2013**, *61*, 4928−4938.
(22) Li, W.; Thirumurugan, A.; Barton, P. T.; Lin, Z.; Henke, S.; Yeung, H. H. M.; Wharmby, M. T.; Bithell, E. G.; Howard, J. A. K.; Cheetham, A. K. *J. Am. Chem. Soc.* **2014**, *136*, 7801−7804.
(23) Asaji, T.; Ito, Y.; Seliger, J.; Zagar, V.; Gradisek, A.; Apih, T. *J. Phys. Chem. A* **2012**, *116*, 12422−12428.
(24) (a) Li, W.; Probert, M. R.; Kosa, M.; Bennett, T. D.; Thirumurugan, A.; Burwood, R. P.; Parinello, M.; Howard, J. A. K.; Cheetham, A. K. *J. Am. Chem. Soc.* **2012**, *134*, 11940−11943. (b) Mączka, M.; Kadłubański, P.; Freire, P. T. C.; Macalik, B.; Paraguassu, W.; Hermanowicz, K.; Hanuza, J. *Inorg. Chem.* **2014**, *53*, 9615−9624.
(25) (a) Nibbering, E. T. J.; Dreyer, J.; Kühn, O.; Bredenbeck, J.; Hamm, P.; Elsaesser, T. *Chem. Phys.* **2007**, *87*, 619−687. (b) Sobczyk, L.; Obrzyd, M.; Filarowski, A. *Molecules* **2013**, *18*, 4467−4476.
(26) Carabatos-Nedelec, C.; Becker, P. *J. Raman Spectrosc.* **1997**, *28*, 663−671.
(27) Maczka, M.; Souza Filho, A. G.; Paraguassu, W.; Freire, P. T. C.; Mendes Filho, J.; Hanuza, J. *Prog. Mater. Sci.* **2012**, *57*, 1335−1381.
(28) (a) Dutler, R.; Rauk, A.; Shaw, R. A. *J. Phys. Chem.* **1990**, *94*, 118−124. (b) Thompson, C. A.; Mowrey, R. C.; Russell, T. P. *J. Mol. Struct.: THEOCHEM* **1999**, *491*, 67−80. (c) Palafox, M. A.; Iza, N.; Gil, M.; Núñez, J. L. *Int. J. Quantum Chem.* **2002**, *89*, 25−47.
(29) Zaporozan, T.; Chen, Z.; Van Wijngaarden, J. *J. Mol. Struct.* **2010**, *264*, 105−110.
(30) Sanchez-Andujar; Gomez-Aguirre, L. C.; Pato Dolan, B.; Yanez-Vilar, S.; Artiga, R.; L. Llamas-Saiz, A. L.; Manna, R. S.; Schnelle, S.; Lang, M.; Ritter, F.; Haghighirad, A. A.; Senaris-Rodrigues, M. A. *CrystEngComm* **2014**, *16*, 3558−3566.
(31) Spencer, E. C.; Kiran, M. S. R. N.; Li, W.; Ramamurty, U.; Ross, N. L.; Cheetham, A. K. *Angew. Chem., Int. Ed.* **2014**, *53*, 5583−5586.